Adsorption (2013) 19:1235–1244
DOI 10.1007/s10450-013-9564-x

Dynamic desorption of CO_2 and CH_4 from amino-MIL-53(Al) adsorbent

Sunil A. Peter · Gino V. Baron · Jorge Gascon · Freek Kapteijn · Joeri F. M. Denayer

Received: 13 March 2013 / Accepted: 23 July 2013 / Published online: 3 August 2013

Abstract Dynamic adsorption–desorption measurements of CO_2 and CH_4 in amino-MIL-53(Al) were carried out in an adsorption breakthrough setup at different temperatures (303, 318, and 333 K) and pressures (1, 5, and 30 bar) to study the desorption dynamics of CO_2 in amino-MIL(Al) as it plays an important role in the design of pressure swing adsorption (PSA) process for the upgrading of biogas. 13X zeolite was used as a reference material. The dynamic adsorption selectivity as well as the desorption efficiency of CO_2 in both amino-MIL-53(Al) and 13X zeolite were calculated to evaluate the potential of amino-MIL-53(Al) for the upgrading of biogas by PSA process.

Keywords Biogas upgrading · Dynamic desorption · Amino-MIL-53(Al) · 13X zeolite

1 Introduction

Global warming due to increased concentrations of greenhouse gases in the atmosphere is of great concern as it is linked to unwanted climate changes (Figueroa et al. 2008; Lashof and Ahuja 1990). Carbon dioxide, methane, nitrous oxide, fluorocarbons, etc., are the major components of greenhouse gases. Even though the amount of CO_2 present in the atmosphere is greater than CH_4, the global warming potential of CH_4 is 21 times higher than that of CO_2 and therefore, the emission of CH_4 to atmosphere must be reduced (Knaebel and Reinhold 2003; Cavenati et al. 2005). The major source of CH_4 to atmosphere is biogas, which is produced under different conditions like anaerobic decomposition of organic matter in municipal digesters, aerobic decomposition of organic residue in solid matter of industrial landfills and fermentation of manure or energy crops (Ryckebosch et al. 2011). Biogas is an alternative source of renewable energy and composed of around 55–70 % CH_4, 30–40 % CO_2 and smaller amounts of NH_3, H_2S, N_2 and hydrocarbons depending on the source of production. Since the biogas contains significant amount of CO_2, its heating value is very low compared to natural gas. To increase the energy content and also to avoid the pipeline and equipment corrosion, the CO_2 content for pipeline grade biomethane should be less than 2–3 % (Delgado et al. 2007). Water scrubbing, amine absorption, membrane separation and adsorption process are the technologies used for the removal of CO_2 to upgrade the biogas.

Adsorption, especially pressure swing adsorption (PSA) or vacuum swing adsorption (VSA) process, is a commercially established process for the separation of gas mixtures in chemical industry (Ruthven et al. 1994; Yang 1997). Hydrogen purification, air separation for nitrogen or oxygen, air drying, olefin-paraffin separation, natural gas upgrading are some of the industrial PSA processes. Desorption dynamics of a strongly adsorbed component plays an important role in the purity and productivity of a PSA process, but most of the studies were focused on the adsorption isotherms or breakthrough curves for the design of the PSA process (Harlick and Tezel 2004; Jain et al. 2003; Rege and Yang 2000; Krishna and Long 2011; Krishna and van Baten 2012). Besides, in any PSA process, the selection of adsorbent is very important for high purity and recovery of the

S. A. Peter · G. V. Baron · J. F. M. Denayer (✉)
Department of Chemical Engineering, Vrije Universiteit Brussel, Brussels, Belgium
e-mail: joeri.denayer@vub.ac.be

J. Gascon · F. Kapteijn
Catalysis Engineering, ChemE, Delft University of Technology, Delft, The Netherlands

product gas. Zeolites, carbon molecular sieves, activated carbon, and silica materials are the adsorbents mainly used for the commercial PSA process. New adsorbents are still needed to optimize these separation processes, and also for the separation of other gaseous systems (for example, flue gas separation for CO_2 capture) to make them commercially more attractive (D'Alessandro et al. 2010).

Metal–organic frameworks (MOFs) have emerged as a new type of functional materials as adsorbents for the separation of various gaseous and liquid systems, and have witnessed explosive development and rapid progress over the past two decades (Li et al. 2009; Hamon et al. 2010; Bao et al. 2011; Herm et al. 2012; Ma 2009). MOFs are inorganic–organic hybrid materials comprised of single metal ions or polynuclear metal clusters linked by organic ligands principally through coordination bonds. An excellent review on CO_2 capture in MOFs was given by Sumida et al. (2012).MOFs with flexible frameworks show breathing effect during adsorption and desorption of guest molecules (Rallapalli et al. 2011; Hamon et al. 2009; Finsy et al. 2009; Biswas et al. 2013; Pera-Titus et al. 2012; Couck et al. 2010). Amino-MIL-53(Al) is an example of a MOF with flexible framework structure, with interesting features for the separation of CO_2 from gas mixtures (Couck et al. 2009; Kim et al. 2012; Stavitski et al. 2011; Boutin et al. 2011). When the pores of this MOF are in the contracted state, they exclude CH_4 of being adsorbed, which results in a very large selectivity in the separation of CO_2 from CH_4.

In the present work, we studied the dynamic desorption of CO_2 from amino-MIL-53(Al) adsorbent. Breakthrough desorption experiments were performed with the adsorbent pre-saturated with a typical biogas composition (Sircar 1988) of 40 % CO_2–60 % CH_4 feed mixture at different temperatures and pressures, and compare the results with well-known 13X zeolite adsorbent.

2 Experimental

2.1 Materials

Amino-MIL-53(Al), synthesized as reported previously (Couck et al. 2012), and 13X zeolite (Si/Al = 1.23) granules (500 μm) supplied by UOP were used as adsorbents. CO_2 (99.995 %), CH_4 (99.95 %), and He (99.995 %) supplied by Air Liquide were used for the adsorption isotherm measurements as well as the breakthrough measurements.

2.2 Adsorption isotherm measurements

Adsorption isotherms were measured in a magnetic suspension gravimetric adsorption setup (Rubotherm GmbH) at 303, 318, and 333 K and up to 40 bar. Prior to the adsorption measurement, around 200 mg of the adsorbent samples was activated under vacuum at a heating rate of 1 K/min up to 473 and 623 K, respectively for amino-MIL-53(Al) and 13X zeolite and kept at that temperature for around 8 h before cooling down to the adsorption temperature. The isotherm temperatures of the samples were controlled using a Julabo thermostat.

2.3 Adsorption–desorption breakthrough measurements

Adsorption–desorption breakthrough measurements were carried out in an in-house built breakthrough set up with a column length of 100 mm and internal diameter of 4.57 mm for both amino-MIL-53(Al) and 13X zeolite. Amino-MIL-53(Al) powder was made into pellets (500–630 μm) by pressing the powder at ca 400 bar pressure in a hydraulic press to form a solid disc, which was crushed and sieved to get the desired pellet fractions. These pellets were activated in situ under helium flow at a heating rate of 5 K/min up to 473 K and kept at that temperature for 4 h before cooling down to the breakthrough experiment temperature. 13X zeolite granules (500 μm) were heated up to 623 K at a heating rate of 5 K/min under helium flow and kept at that temperature for 6 h before cooling down to adsorption temperature. Around 715 mg of amino-MIL-53(Al) and 972 mg of 13X zeolite were used for the breakthrough experiments. Adsorption–desorption breakthrough experiments were carried out at 1, 5, and 30 bar for amino-MIL-53(Al) and, at 1 and 5 bar for 13X zeolite. 40 % CO_2 and 60 % CH_4 at a total flow of 20 Nml/min was used as the feed mixture for all the adsorption breakthrough measurements and 20 Nml/min of He purge was used for the dynamic desorption measurements. For the breakthrough measurements at 1 bar, the adsorbent column outlet was directly open to the atmosphere and a portion of the outlet flow was passed through an online mass spectrometer (MS) to monitor the outlet concentration. The outlet flow was diluted with nitrogen flow before connecting to the MS, in order to get a linear response of the outlet flow. For the breakthrough measurements at high pressures (5 and 30 bar), the outlet of the adsorbent column was connected to a backpressure regulator to maintain the particular adsorption pressures inside the column. A mass flow meter was also connected before the back pressure regulator to measure the exact outlet flow rate from the column and a small portion of this outlet flow was connected through a 50 μ capillary to the online MS to measure the outlet concentration. From the outlet concentration and outlet flow rate, the flow rates of individual components were calculated. The adsorption and desorption breakthrough measurements were carried out at 303, 318, and 333 K and in some cases, the desorption was carried out by increasing the column temperature at a rate

of 5 K/min up to 473 K under He flow to desorb the adsorbed molecules easily.

The amount adsorbed of component a, q_a was calculated as:

$$q_a = \frac{(F\tau_a - \varepsilon VP/RT)x_a}{m_{ads}}$$

where F is the total flow rate (mmol/min); τ_a is the mean residence time (min); ε is the total adsorbent column porosity; V is volume of the column (ml); m_{ads} is the mass of the adsorbent (g); P is the total pressure inside the column (bar); x_a is the mole fraction of component a in the gas phase; R is the ideal gas constant (8.31×10^{-2} ml bar K^{-1} $mmol^{-1}$); and T is the column temperature (K). The mean residence time for adsorption breakthrough was calculated as:

$$\tau_a = \int_0^{t_\infty} \left(1 - \frac{F_a}{F_{ao}}\right) dt$$

where F_a is the outlet flow rate of component a; and F_{ao} is the feed flow rate of component a. The mean residence time for the desorption breakthrough curve was calculated as:

$$\tau_a = \int_0^{t_\infty} \left(\frac{F_a}{F_{ao}}\right) dt$$

The mean residence time was corrected for the dead volume caused by the tubing and fittings of the breakthrough setup. Both pure component selectivity (calculated from the pure component isotherms) as well as dynamic binary adsorption selectivity (from breakthrough measurements) $\alpha_{a/b}$, of component a over component b were calculated as (Myers and Prausnitz 1965):

$$\alpha_{a/b} = \frac{q_a/x_a}{q_b/x_b}$$

where q_a and q_b are amount of components a and b adsorbed, and x_a and x_b are the mole fractions of components a and b in the gas phase at a particular feed pressure.

The adsorption selectivity can also be calculated from the initial slope of the adsorption isotherm as (Myers and Prausnitz 1965):

$$\alpha_{a/b} = \frac{K_a}{K_b}$$

where K_a an K_b are the initial slopes of the adsorption isotherms (Henry's law constant) of component a and b, respectively.

3 Results and discussion

The adsorption and desorption isotherms of CO_2 and CH_4 in amino-MIL-53(Al) were measured at different temperatures up to 40 bar pressure as shown in Fig. 1. The CO_2 adsorption capacity at 303 K reached a plateau initially around 5 bar and again increased around 10 bar pressure and reached a second plateau around 40 bar. The desorption isotherm branch at 303 K showed a large hysteresis and met back the adsorption isotherm around 3 bar. In the previous study (Couck et al. 2009) the second adsorption plateau was around 20 bar pressure and the adsorption capacity was also less than the present value. The previous equilibrium adsorption isotherms were measured by volumetric method whereas; the present measurements were carried out using gravimetric method. The amino-MIL-53(Al) from different batches as well as the difference in the measurement methods may contribute to the higher adsorption capacity of CO_2 in the present study. Moreover, the crystal size ($\sim$1 μm) of the present sample was higher than that of the previous sample, which may contribute to the large hysteresis in desorption isotherm. At 318 and 333 K, the CO_2 adsorption capacity from the first adsorption plateau started to increase around 20 bar and may take much higher pressure than 40 bar to reach the second plateau. The CO_2 adsorption capacities in amino-MIL-53(Al) at 5 bar were 2.40, 2.16, and 2.01 mmol/g, respectively for 303, 318, and 333 K. But at 40 bar, the CO_2 adsorption capacities showed huge difference with values of 7.73, 4.37, and 3.49 mmol/g, respectively for 303, 318, and 333 K. For CH_4 adsorption isotherms, there was negligible adsorption initially and the adsorption capacity started to increase when the pressure was greater than 1 bar. The CH_4 adsorption capacities at 40 bar were 3.14, 2.50, and 2.32 mmol/g, respectively for 303, 318, and 333 K. CH_4 isotherm also showed hysteresis during desorption. The amino-MIL-53(Al) is a flexible MOF with distinct crystallographic structures at room temperature; one with narrow pore (*np*) and another with large pore (*lp*) framework (Stavitski et al. 2011; Boutin et al. 2011). The transition from *np* to *lp* is induced by guest molecules adsorbed inside the pores. Recent in situ XRD measurements showed that, at low pressure amino-MIL-53(Al) was in a very narrow pore form (*vnp*) and the guest molecule adsorption at low pressure transformed this structure to the *np* form (Couck et al. 2012). At much higher pressure the transition from *np* to *lp* has occurred. The pore sizes obtained from XRD measurements were approximately 13.70 × 2.68 Å for *vnp*, 13.47 × 3.00 Å for *np*, and 11.10 × 8.84 Å for *lp* framework structures. This very narrow pore form at low pressure is responsible for the exclusion of CH_4 at <1 bar pressure. The pure component CO_2 adsorption capacity of amino-MIL-53(Al) at 1 bar partial pressure and 303 K (ca 1.96 mmol/g) was higher than the CO_2 adsorption capacities reported for commercial adsorbents, which are used for the kinetic separation of CO_2 and CH_4, like carbon molecular sieve, Takeda

CMS3K (ca 1.87 mmol/g at 1 bar and 298 K) (Cavenati et al. 2005) and Molecular Gate® Sr-ETS-4 (ca 1.1 mmol/g at 1 bar and 298 K) (Mitariten 2001; Primera-Pedrozo et al. 2010).

The adsorption and desorption isotherms of CO_2 and CH_4 in 13X zeolite at different temperatures and pressure up to 40 bar are shown in Fig. 2. The CO_2 adsorption reached a plateau around 10 bar, but CH_4 adsorption kept on increasing till 40 bar. The initial uptake of CO_2 in 13X zeolite was very steep at low pressure compared to CH_4 adsorption. The desorption of CO_2 from 13X zeolite was completely reversible with a very small hysteresis, while the CH_4 desorption was completely reversible without any hysteresis. The strong electrostatic interaction of CO_2 with extra-framework Na^+ present inside the cavity of 13X zeolite may cause this hysteresis, while the electrostatic interaction of CH_4 with Na^+ is weak compared to the interaction of CO_2 with Na^+ ion (Pillai et al. 2012; Cavenati et al. 2004). The isosteric heat of adsorption of CO_2 (calculated using Clausius–Clapeyron equation (Pillai et al. 2012) was ca −43 kJ/mol in zeolite 13X, whereas it was ca −32 kJ/mol in amino-MIL-53(Al). The isosteric heat of CH_4 adsorption was less in both amino-MIL-53(Al) (−20 kJ/mol) and zeolite 13X (−22 kJ/mol; all values were calculated at 1 mmol/g of pure component adsorbed).

The adsorption–desorption breakthrough curves of 40 % CO_2–60 % CH_4 gas mixture at 303, 318, and 333 K were measured in amino-MIL-53(Al) at a total feed pressure of 1, 5, and 30 bar. Figure 3 shows the adsorption–desorption breakthrough measurements at 1 bar and different temperatures in amino-MIL-53(Al) adsorbent column. CH_4 adsorption breakthrough occurred at almost the same time for all the temperature conditions and there was no roll-up in the CH_4 curve, which indicates that practically no CH_4 adsorbed in amino-MIL-53(Al). The CO_2 breakthrough time decreased with increase in adsorption temperature and the total amount of CO_2 was similar to the amount adsorbed in pure component CO_2 isotherm at the particular partial pressure and temperatures as shown in Table 1. The amount of CH_4 adsorbed was practically nil at 1 bar breakthrough measurement. The desorption of this saturated amino-MIL-53(Al) column was carried out at isothermal conditions of 303, 318, and 333 K, respectively, by purging the column at 1 bar with He at a flow rate of 20 Nml/min. The CH_4 present in the void space of the column came out very fast and CO_2 also desorbed completely with much ease and low dispersion at higher temperature. Figure 4 shows the adsorption–desorption breakthrough measurements of 40 % CO_2–60 % CH_4 gas mixture at 5 bar and different isothermal conditions in amino-MIL-53(Al) column. At 303 K, CH_4 initially adsorbed in the adsorbent and was then replaced by CO_2, which is shown as a roll-up in the CH_4 breakthrough curve. With increase in temperature, the CH_4 roll-up in the breakthrough curve also decreased, which means that the amount of adsorbed CH_4 replaced with CO_2 decreased with increase in temperature. The amount of CH_4 adsorbed was comparable at all these three temperatures with a value of around 0.18 mmol/g, which was higher than the values obtained from pure component adsorption isotherm of CH_4 in amino-MIL-53(Al) at these temperatures and partial pressure as shown in Table 1. This increase in CH_4 co-adsorption capacity could be due to the transition of amino-MIL-53(Al) framework structure from *vnp* to *np* form in the presence of CO_2 at this partial pressure (Couck et al. 2012) and which in turn increased the co-adsorption of CH_4 in amino-MIL-53 (Al). CH_4 desorbed very rapidly during the dynamic desorption by He purge at 5 bar (Fig. 4b). Desorption of CO_2 was also complete at isothermal conditions, but with a large dispersion at low temperature (303 K). The huge initial peak in the desorption breakthrough curves of CH_4 and CO_2 was due to the sudden release of adsorbed CO_2 and CH_4 by sudden decrease in CO_2 and CH_4 partial pressures when He flow enters the adsorbent column. Figure 5 shows the dynamic adsorption and desorption breakthrough curves at 30 bar for 40 % CO_2–60 % CH_4 gas mixture in amino-MIL-53(Al) column at 303, 318, and 333 K. At 30 bar, significant amount of CH_4 co-adsorbed in amino-MIL-53(Al) as the time lag between the CH_4 and CO_2 breakthrough curves decreased

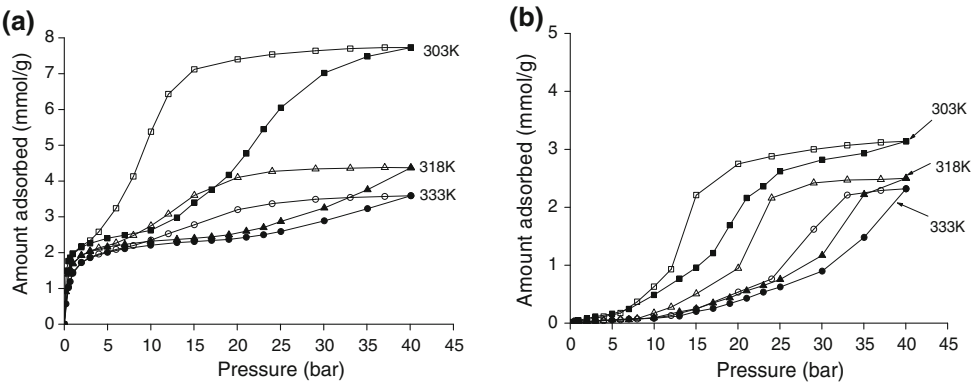

Fig. 1 Adsorption and desorption isotherms of (**a**) CO_2 and (**b**) CH_4 in amino-MIL-53(Al) at different temperatures (*closed symbol* for adsorption and *open symbol* for desorption)

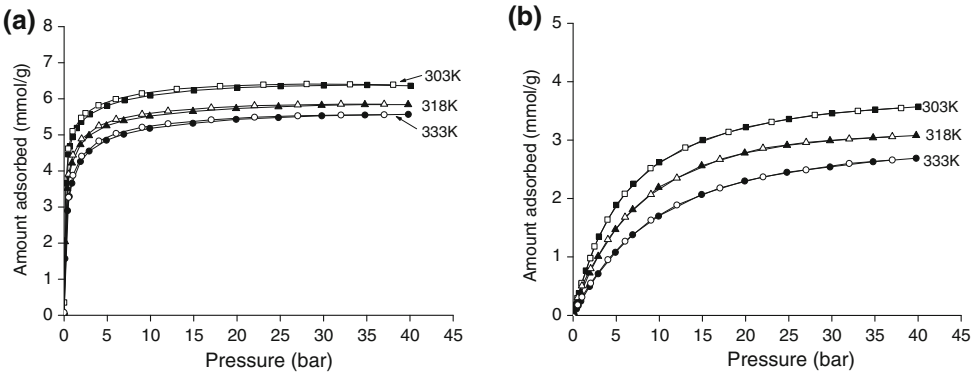

Fig. 2 Adsorption and desorption isotherms of (**a**) CO_2 and (**b**) CH_4 in 13X zeolite at different temperatures (*closed symbol* for adsorption and *open symbol* for desorption)

compared to the low-pressure breakthrough curves. The adsorption breakthrough curve of CO_2 at 303 K showed significant dispersion compared to the adsorption breakthrough curves at 318 and 333 K. This is attributed to the transition of framework from *np* form to *lp* form at this high total pressure and the lower isotherm steepness in this form at high pressure (Fig. 1). The dynamic adsorption capacities of CO_2 at 303, 318, and 333 K were almost the same compared to the pure component isotherm values at the respective CO_2 partial pressure of feed composition (Table 1). However, the amount of co-adsorbed CH_4 was significantly higher compared to the pure component adsorption isotherm values at the particular CH_4 partial pressure of the feed composition, due to the framework transition in presence of higher CO_2 partial pressure in the feed. Desorption of CH_4 and CO_2 were carried at 30 bar by purging with He at a flow rate of 20 Nml/min. CH_4 desorbed completely and CO_2 seemed to be desorbed almost completely after about 45 min. But in fact, around 82, 74, and 84 % of the adsorbed CO_2 only desorbed, respectively at 303, 318, and 333 K and, the remaining amount was trapped inside the adsorbent due to the desorption hysteresis at isothermal conditions. We could release this trapped CO_2 by heating the column as shown in Fig. 6.

For comparison purposes, the adsorption–desorption breakthrough curves of 40 % CO_2–60 % CH_4 feed mixture at 303, 318, and 333 K were measured in 13X zeolite, also at a total pressure of 1 and 5 bar. Figure 7 shows the dynamic adsorption–desorption curves of CO_2–CH_4 feed mixture at 1 bar feed pressure and different isothermal conditions. CH_4 came through the column first, because of low adsorption capacity for CH_4 in 13X zeolite compared to CO_2 and showed a roll-up, which was caused by the desorption of pre-adsorbed CH_4 by the advancing CO_2 concentration front along the adsorbent column. CO_2 replaced the adsorbed CH_4 almost completely as the amount of CH_4 adsorbed calculated from the breakthrough curves were negligible at 1 bar as shown in Table 2. Desorption of CO_2 and CH_4 from 13X zeolite column was carried by purging with 20 Nml/min of He gas at isothermal conditions of 303, 318, and 333 K and 1 bar. CH_4 from the void space and a little bit adsorbed in the adsorbent came out rapidly while desorption of CO_2 was difficult as the CO_2 desorption curve spread out over a very long period (Fig. 7b). To make CO_2 desorption from 13X zeolite faster and complete, we may heat the column simultaneously along with He purge as shown in Fig. 8. Figure 9 shows the adsorption–desorption breakthrough curves of 40 % CO_2–60 % CH_4 gas mixture in 13X zeolite at 5 bar pressure and different isothermal conditions. Both CH_4 and CO_2 adsorption breakthrough curves were very steep and CH_4 adsorption breakthrough curves showed very large roll-up. At 5 bar also, significant amount of pre-adsorbed CH_4 was replaced by the advancing CO_2 concentration front along the adsorbent column. The net amount of CH_4 adsorbed on 13X zeolite was very low compared to pure component isotherm adsorption capacities of CH_4 at particular partial pressure and temperature (Table 2). In competitive conditions, strong CO_2 adsorption leads to negligible CH_4 adsorption. The desorption of adsorbed CH_4 and CO_2 was carried out at respective isothermal conditions by purging the column with 20 Nml/min of He at 5 bar. CH_4 desorbed completely from the column very rapidly, but the desorption of CO_2 was very difficult, with large dispersion in the desorption breakthrough curve (Fig. 9b). In order to remove CO_2 completely from 13X zeolite, we may need to heat the adsorbent column as shown in Fig. 10. The desorption was carried out initially at isothermal condition of 303 K by purging with He at a flow rate of 20 Nml/min during 55 min followed by an increase in temperature at a rate of 5 K/min up to 473 K.

Both pure component adsorption selectivity (calculated from the pure component isotherms) as well as dynamic binary adsorption selectivity (from breakthrough measurement) were calculated and shown in Table 3. It should be stressed that in a PSA process, the effective loading or working capacity of an adsorbent depends on the adsorption and desorption conditions and therefore, Rege and Yang (2001) have defined a separation factor for a binary gas mixture, based on the isothermal working capacities and initial slopes of the adsorption isotherms of the

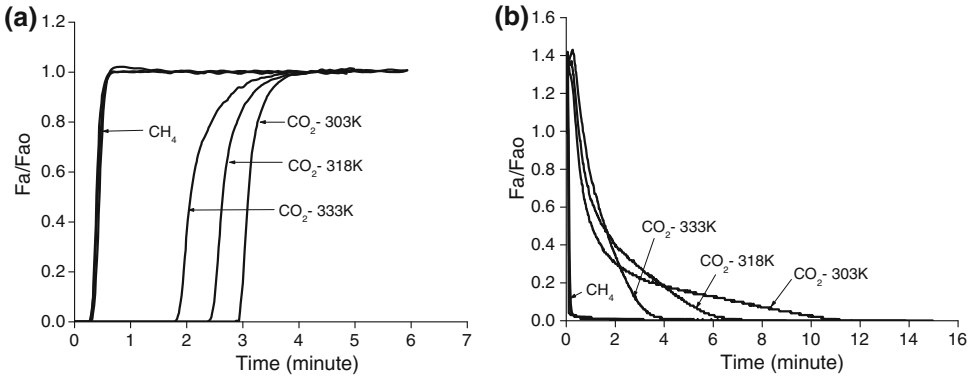

Fig. 3 (**a**) Adsorption and (**b**) desorption breakthrough curves of 40 % CO_2–60 % CH_4 in amino-MIL-53(Al) column at 1 bar and different temperatures (feed flow rate = 20 Nml/min; desorption by He purging at a flow rate of 20 Nml/min at 1 bar)

Table 1 Equilibrium adsorption capacities of CO_2 and CH_4 in amino-MIL-53(Al) calculated from pure component adsorption isotherms and adsorption breakthrough curves at different temperatures for a feed composition of 40 % CO_2–60 % CH_4 at a total pressure of 1, 5, and 30 bar

Gas	Total pressure (bar)	Partial pressure (bar)	Amount adsorbed (mmol/g)					
			Isotherm			Breakthrough		
			303 K	318 K	333 K	303 K	318 K	333 K
CO_2	1	0.4	1.68	1.30	0.90	1.38	1.17	0.92
	5	2.0	2.15	1.92	1.72	2.29	2.07	1.82
	30	12.0	2.86	2.36	2.26	2.87	2.57	2.36
CH_4	1	0.6	0.04	0.02	0.01	0.01	0.00	0.00
	5	3.0	0.14	0.05	0.04	0.18	0.18	0.17
	30	18.0	1.44	0.41	0.30	2.66	2.00	1.20

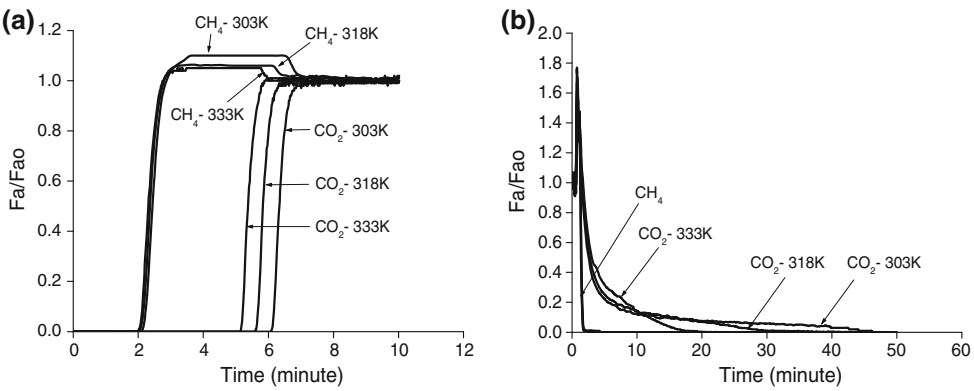

Fig. 4 (**a**) Adsorption and (**b**) desorption breakthrough curves of 40 % CO_2–60 % CH_4 in amino-MIL-53(Al) column at 5 bar and different temperatures (feed flow rate = 20 Nml/min; desorption by He purging at a flow rate of 20 Nml/min at 5 bar)

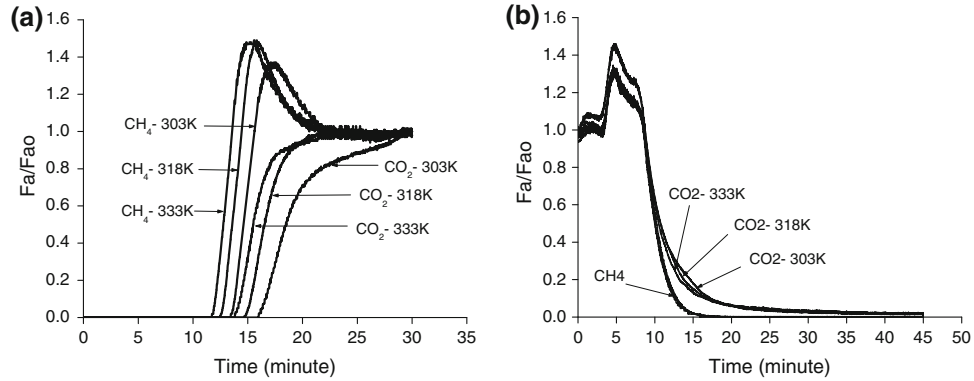

Fig. 5 (**a**) Adsorption and (**b**) desorption breakthrough curves of 40 % CO_2–60 % CH_4 in amino-MIL-53(Al) column at 30 bar and different temperatures (feed flow rate = 20 Nml/min; desorption by He purging at a flow rate of 20 Nml/min at 30 bar)

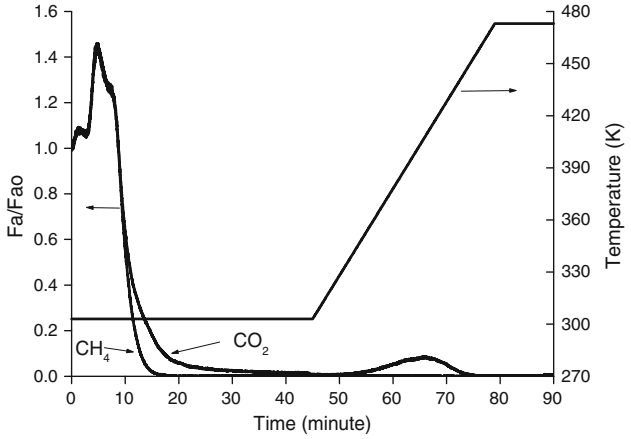

Fig. 6 Desorption curves of CH_4 and CO_2 at 30 bar in amino-MIL-53(Al) initially at isothermal condition of 303 K and then heated at a rate of 5 K/min up to 473 K (desorption by He purge at a flow rate of 20 Nml/min at 30 bar)

components present in the gas mixture. Since in actual PSA processes, the temperature inside the adsorbent column changes during adsorption–desorption cycles, Ackley (2000) has defined a separation factor as the ratio of adiabatic working capacities of two components in the binary gas mixture. In this work, dynamic desorption was performed using He at the same pressure as that of the adsorption breakthrough experiment, such that these more realistic separation factors could not be calculated. Using more simple definitions of selectivity, we mainly want to highlight the different behavior of both materials. At 1 bar total pressure, amino-MIL-53(Al) exhibits almost infinite selectivity for CO_2 over CH_4. However, at 5 and 30 bar, amino-MIL-53(Al) displayed lower breakthrough adsorption selectivity than the pure component equilibrium adsorption isotherm selectivity due to high co-adsorption of CH_4 in the presence of CO_2. 13X zeolite showed lower dynamic adsorption selectivity than amino-MIL-53(Al) for CO_2 over CH_4 at 1 bar for all the three temperatures, but at 5 bar its selectivity surmounts that of amino-MIL-53 due to more efficient displacement of adsorbed CH_4 by the advancing CO_2 concentration front along the column. At 1 bar pressure, amino-MIL-53(Al) showed shape selectivity for CO_2 due to the exclusion of CH_4, as it stays in *vnp* form at low pressure region. In 13X zeolite, the strong electrostatic interaction of CO_2 caused the displacement of weakly adsorbed CH_4, which in turn increased the dynamic adsorption selectivity in 13X zeolite. As expected, the adsorption selectivity calculated using the initial slope (Henry's law constant) of the pure component adsorption isotherms showed higher values [35, 57, and 62, respectively for 13X zeolite at 303, 318, and 333 K; 143, 335, and 226, respectively for amino-MIL-53(Al) at 303, 318, and 333 K] compared to the selectivity values calculated using equilibrium amount of pure component adsorbed in the pure component adsorption isotherms at particular

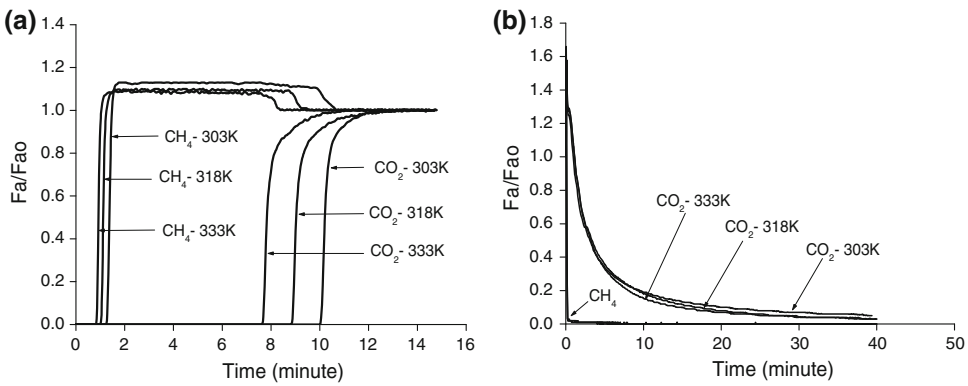

Fig. 7 (**a**) Adsorption and (**b**) desorption breakthrough curves of 40 % CO_2–60 % CH_4 in 13X zeolite column at 1 bar and different temperatures. (feed flow rate = 20 Nml/min; desorption by He purging at a flow rate of 20 Nml/min at 1 bar)

Table 2 Equilibrium adsorption capacities of CO_2 and CH_4 in 13X zeolite calculated from pure component isotherms and adsorption breakthrough curves at different temperatures for a feed composition of 40 % CO_2–60 % CH_4 at a total pressure of 1 and 5 bar

Gas	Total pressure (bar)	Partial pressure (bar)	Amount adsorbed (mmol/g)					
			Isotherm			Breakthrough		
			303 K	318 K	333 K	303 K	318 K	333 K
CO_2	1	0.4	4.27	3.52	2.98	4.13	3.55	3.06
	5	2.0	5.35	4.76	4.30	5.26	4.89	4.48
CH_4	1	0.6	0.33	0.26	0.17	0.07	0.07	0.06
	5	3.0	1.35	1.03	0.73	0.12	0.14	0.14

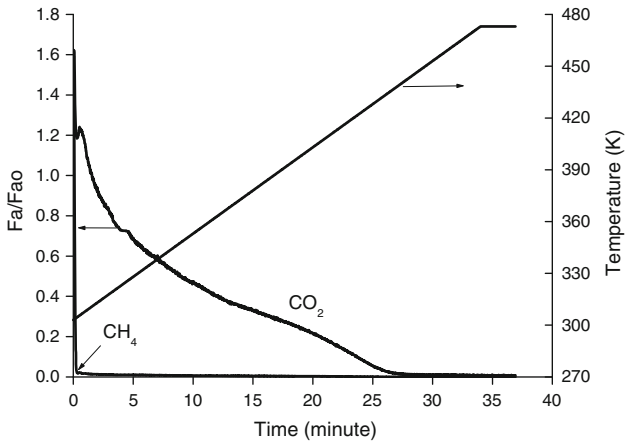

Fig. 8 Dynamic desorption of CH_4 and CO_2 from 13X zeolite column by heating at a rate of 5 K/min, starting from 303 to 473 K (feed composition 40 % CO_2–60 % CH_4; feed flow rate 20 Nml/min; He purge flow rate 20 Nml/min at 1 bar)

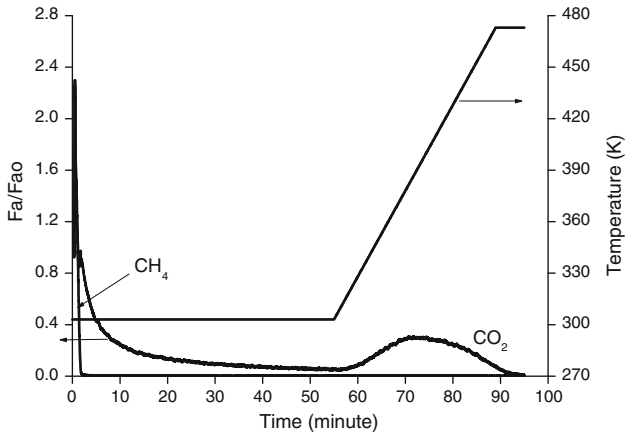

Fig. 10 Desorption curves of CH_4 and CO_2 at 5 bar in 13X zeolite initially at isothermal condition of 303 K and heated at a rate of 5 K/min to 473 K (desorption by He purge at a flow rate of 20 Nml/min at 5 bar)

partial pressures. However, these initial adsorption selectivity values are still lower than the values calculated using equilibrium amount adsorbed in the dynamic binary breakthrough test at low pressure (1 bar).

Table 4 shows the dynamic CO_2 desorption efficiency (under isothermal purging with He) in amino-MIL-53(Al) and 13X zeolite in terms of percentage CO_2 desorbed for a period of 3 times the breakthrough time of CO_2 in both these materials. Desorption of CO_2 was very efficient in amino-MIL-53(Al) at isothermal conditions compared to 13X zeolite at both 1 and 5 bar. At 303 K, the amount CO_2 desorbed was around 94 % in amino-MIL-53(Al) and at higher temperatures, desorption of CO_2 was complete within the particular desorption time. The desorption efficiency was low in 13X zeolite at isothermal conditions due to strong adsorption of CO_2. Only 65 % of the adsorbed of

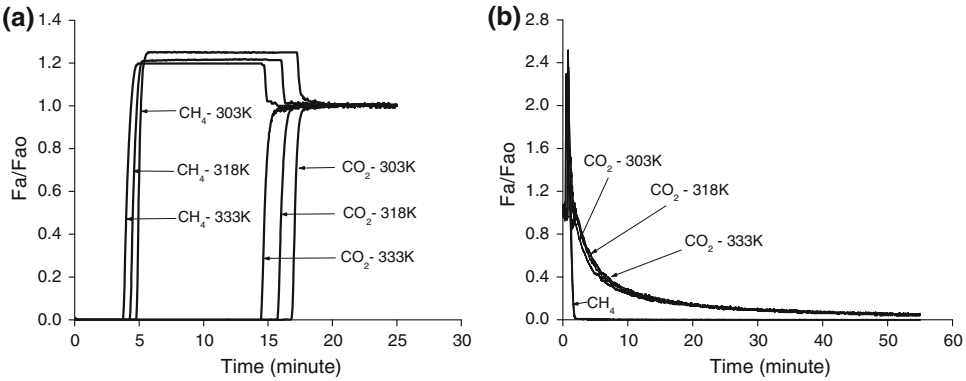

Fig. 9 (**a**) Adsorption and (**b**) desorption breakthrough curves of 60 % CH_4 and 40 % CO_2 in 13X zeolite column at 5 bar and different temperatures (feed flow rate 20 Nml/min; He purge flow rate 20 Nml/min at 5 bar)

Table 3 Both pure component (isotherm) and binary (breakthrough) adsorption selectivities of CO_2 over CH_4 for a feed mixture of 40 % CO_2–60 % CH_4 at different temperatures and a feed pressure of 1, 5, and 30 bar in amino-MIL-53(Al) and, 1 and 5 bar in 13X zeolite

Adsorbent	Total pressure (bar)	Selectivity, α_{CO_2/CH_4}					
		Isotherm			Breakthrough		
		303 K	318 K	333 K	303 K	318 K	333 K
Amino-MIL-53(Al)	1	63	98	135	207	∞	∞
	5	23	58	64	19	17	16
	30	3	9	11	2	2	3
13X	1	19	20	26	88	76	76
	5	6	7	9	66	52	48

Table 4 Percentage of total CO_2 desorbed at different pressure and temperature for a period of 3 times the CO_2 breakthrough time in amino-MIL-53(Al) and 13X zeolite

Adsorbent	Total pressure (bar)	CO_2 breakthrough time (min)			Amount of CO_2 desorbed at 3 times the breakthrough time (%)		
		303 K	303 K	318 K	303 K	303 K	318 K
Amino-MIL-53(Al)	1	2.9	2.4	1.8	94	100	100
	5	6.1	5.6	5.2	70	85	98
	30	16.0	14.8	13.9	82	74	84
13X	1	10.0	8.8	7.6	65	69	73
	5	16.8	15.7	14.4	55	63	68

CO_2 could desorb by isothermal purging with He at 303 K and 1 bar. At higher temperatures, the CO_2 desorption efficiency increased in zeolite 13X. Since the desorption of CO_2 is much easier in amino-MIL-53(Al), a simple PSA process (with purging to regenerate the adsorbent) may be possible for bulk CO_2/CH_4 separation using amino-MIL-53(Al) adsorbent. However, for 13X zeolite, temperature swing adsorption (TSA) or vacuum sing adsorption (VSA) processes may be suited for CO_2/CH_4 separation due to strong adsorption and the difficulty in desorption of CO_2 from 13X zeolite by simple purging.

4 Conclusions

Amino-MIL-53-(Al) displayed almost infinite dynamic breakthrough adsorption selectivity of CO_2 over CH_4 for a feed mixture of 40 % CO_2–60 % CH_4 at 1 bar pressure. However, the breakthrough selectivity for CO_2 over CH_4 was less than the pure component adsorption isotherm selectivity at 5 and 30 bar due to significant co-adsorption of CH_4 in the presence of CO_2 at these pressures. The breakthrough adsorption selectivity of CO_2 over CH_4 in 13X zeolite was higher than the pure component adsorption isotherm selectivity at both 1 and 5 bar. 13X zeolite displayed very high capacity for CO_2, but the desorption of CO_2 was difficult with large spread out in the desorption breakthrough curve even at 1 bar. Even though the CO_2 adsorption capacity was lower in amino-MIL-53(Al) than 13X zeolite, the higher desorption efficiency makes it a potential adsorbent for the upgrading of biogas at low feed pressure.

Acknowledgments S. A. Peter is grateful to Belgium Science Policy Office (BELPSO) and the Marie Curie Actions of the European Commission for financial support in the form of post-doctoral fellowship.

References

Ackley, M.W.: Multilayer adsorbent beds for PSA gas separation. U. S. Patent 6,152,991 (2000)

Bao, Z., Yu, L., Ren, Q., Lu, X., Deng, S.: Adsorption of CO_2 and CH_4 on a magnesium-based metal organic framework. J. Colloid Interface Sci. **353**, 549–556 (2011)

Biswas, S., Rémy, T., Couck, S., Denysenko, D., Rampelberg, G., Denayer, J.F.M., Volkmer, D., Detavernier, C., Voort, P.V.D.: Partially fluorinated MIL-47 and Al-MIL-53 frameworks: influence of functionalization on sorption and breathing properties. Phys. Chem. Chem. Phys. **15**, 3552–3561 (2013)

Boutin, A., Couck, S., Coudert, F.X., Serra-Crespo, P., Gascon, J., Kapteijn, F., Fuchs, A.H., Denayer, J.F.M.: Thermodynamic analysis of the breathing of amino-functionalized MIL-53(Al) upon CO_2 adsorption. Microporous Mesoporous Mater. **140**, 108–113 (2011)

Cavenati, S., Carlos, A., Rodrigues, A.: Upgrade of methane from landfill gas by pressure swing adsorption. Energy Fuels **19**, 2545–2555 (2005)

Cavenati, S., Grande, C.A., Rodrigues, A.E.: Adsorption equilibrium of methane, carbon dioxide, and nitrogen on zeolite 13× at high pressures. J. Chem. Eng. Data **49**, 1095–1101 (2004)

Couck, S., Denayer, J.F.M., Baron, G.V., Rémy, T., Gascon, J., Kapteijn, F.: An amine-functionalized MIL-53 metal–organic framework with large separation power for CO_2 and CH_4. J. Am. Chem. Soc. **131**, 6326–6327 (2009)

Couck, S., Gobechiya, E., Kirschhock, C.E.A., Serra-Crespo, P., Juan-Alcañiz, J., Martinez Joaristi, A., Stavitski, E., Gascon, J., Kapteijn, F., Baron, G.V., Denayer, J.F.M.: Adsorption and separation of light gases on an amino-functionalized metal–organic framework: an adsorption and in situ XRD study. ChemSusChem **5**, 740–750 (2012)

Couck, S., Rémy, T., Baron, G.V., Gascon, J., Kapteijn, F., Denayer, J.F.M.: A pulse chromatographic study of the adsorption properties of the amino-MIL-53 (Al) metal–organic framework. Phys. Chem. Chem. Phys. **12**, 9413–9418 (2010)

D'Alessandro, D.M., Smit, B., Long, J.R.: Carbon dioxide capture: prospects for new materials. Angew. Chem. Int. Ed. **49**, 6058–6082 (2010)

Delgado, J.A., Uguina, M.A., Sotelo, J.L., Ruiz, B., Rosario, M.: Carbon dioxide/methane separation by adsorption on sepiolite. J. Nat. Gas Chem. **16**, 235–243 (2007)

Figueroa, J.D., Fout, T., Plasynski, S., McIlvried, H., Srivastava, R.D.: Advances in CO_2 capture technology—The U.S. Department of Energy's Carbon Sequestration Program. Int. J. Greenh. Gas Control **2**, 9–20 (2008)

Finsy, V., Ma, L., Alaerts, L., De Vos, D.E., Baron, G.V., Denayer, J.F.M.: Separation of CO_2/CH_4 mixtures with the MIL-53(Al) metal–organic framework. Microporous Mesoporous Mater. **120**, 221–227 (2009)

Hamon, L., Jolimaître, E., Pirngruber, G.: CO_2 and CH_4 separation by adsorption using Cu–BTC metal–organic framework. Ind. Eng. Chem. Res. **49**, 7497–7503 (2010)

Hamon, L., Llewellyn, P.L., Devic, T., Ghoufi, A., Clet, G., Guillerm, V., Pirngruber, G.D., Maurin, G., Serre, C., Driver, G., Beek, W.V., Jolimaître, E., Vimont, A., Daturi, M., Férey, G.: Co-adsorption and separation of CO_2–CH_4 mixtures in the highly flexible MIL-53(Cr) MOF. J. Am. Chem. Soc. **53**, 17490–17499 (2009)

Harlick, P.J.E., Tezel, F.H.: An experimental adsorbent screening study for CO_2 removal from N_2. Microporous Mesoporous Mater. **76**, 71–79 (2004)

Herm, Z.R., Krishna, R., Long, J.R.: Reprint of: CO_2/CH_4, CH_4/H_2 and $CO_2/CH_4/H_2$ separations at high pressures using Mg_2(dobdc). Microporous Mesoporous Mater. **157**, 94–100 (2012)

Jain, S., Moharir, A.S., Li, P., Wozny, G.: Heuristic design of pressure swing adsorption: a preliminary study. Sep. Purif. Technol. **33**, 25–43 (2003)

Kim, J., Kim, W.Y., Ahn, W.S.: Amine-functionalized MIL-53(Al) for CO_2/N_2 separation: effect of textural properties. Fuel **102**, 574–579 (2012)

Knaebel, K., Reinhold, H.: Landfill gas: from rubbish to resource. Adsorption **9**, 87–94 (2003)

Krishna, R., van Baten, J.M.: A comparison of the CO_2 capture characteristics of zeolites and metal–organic frameworks. Sep. Purif. Technol. **87**, 120–126 (2012)

Krishna, R., Long, J.R.: Screening metal–organic frameworks by analysis of transient breakthrough of gas mixtures in a fixed bed adsorber. J. Phys. Chem. C **115**, 12941–12950 (2011)

Lashof, D.A., Ahuja, D.R.: Relative contributions of greenhouse gas emissions to global warming. Nature **344**, 529–531 (1990)

Li, J.R., Kuppler, R.J., Zhou, H.C.: Selective gas adsorption and separation in metal–organic frameworks. Chem. Soc. Rev. **38**, 1477–1504 (2009)

Ma, S.: Gas adsorption applications of porous metal–organic frameworks. Pure Appl. Chem. **81**, 2235–2251 (2009)

Mitariten, M.: New technology improves nitrogen-removal economics. Oil Gas J. **99**, 42–44 (2001)

Myers, A.L., Prausnitz, J.L.: Thermodynamics of mixed-gas adsorption. AIChE J. **11**, 121–127 (1965)

Pera-Titus, M., Lescouet, T., Aguado, S., Farrusseng, D.: Quantitative characterization of breathing upon adsorption for a series of amino-functionalized MIL-53. J. Phys. Chem. C **116**, 9507–9516 (2012)

Pillai, R.S., Peter, S.A., Jasra, R.V.: CO_2 and N_2 adsorption in alkali metal ion exchanged X-Faujasite: grand canonical Monte Carlo simulation and equilibrium adsorption studies. Microporous Mesoporous Mater. **162**, 143–151 (2012)

Primera-Pedrozo, J.N., Torres-Cosme, B.D., Clardy, M.E., Rivera-Ramos, M.E., Hernández-Maldonado, A.J.: Titanium silicate porous materials for carbon dioxide adsorption: synthesis using a structure directing agent, detemplation and inclusion of alkaline earth metal cations. Ind. Eng. Chem. Res. **49**, 7515–7523 (2010)

Rallapalli, P., Prasanth, K.P., Patil, D., Somani, R.S., Jasra, R.V., Bajaj, H.C.: Sorption studies of CO_2, CH_4, N_2, CO, O_2 and Ar on nanoporous aluminum terephthalate. J. Porous Mater. **18**, 205–210 (2011)

Rege, S.U., Yang, R.T.: Kinetic separation of oxygen and argon using molecular sieve carbon. Adsorption **22**, 15–22 (2000)

Rege, S.U., Yang, R.T.: A simple parameter for selecting an adsorbent for gas separation by pressure swing adsorption. Sep. Sci. Technol. **36**, 3355–3365 (2001)

Ruthven, D.M., Farooq, S., Knaebel, K.S.: Pressure swing adsorption. Wiley-VCH, New York (1994)

Ryckebosch, E., Drouillon, M., Vervaeren, H.: Techniques for transformation of biogas to biomethane. Biomass Bioenergy **35**, 1633–1645 (2011)

Sircar, S.: Separation of methane and carbon dioxide gas mixtures by pressure swing adsorption. Sep. Sci. Technol. **23**, 519–529 (1988)

Stavitski, E., Pidko, E.A., Couck, S., Remy, T., Hensen, E.J.M., Weckhuysen, B.M., Denayer, J., Gascon, J., Kapteijn, F.: Complexity behind CO_2 capture on NH_2-MIL-53(Al). Langmuir **53**, 3970–3976 (2011)

Sumida, K., Rogow, D.L., Mason, J.A., McDonald, T.M., Bloch, E.D., Herm, Z.R., Bae, T., Long, J.R.: Carbon dioxide capture in metal–organic frameworks. Chem. Rev. **112**, 724–781 (2012)

Yang, R.T.: Gas separation by adsorption process. Imperial College Press, London (1997)